



Kent Academic Repository

Walters, J.K., Fox, D.M., Burke, Terry, Weedon, O.D., Newport, Robert J. and Howells, W.S. (1994) *The Effect Of Temperature On The Structure Of Amorphous Hydrogenated Carbon*. *Journal of Chemical Physics*, 101 (5). pp. 4288-4300. ISSN 0021-9606.

Downloaded from

<https://kar.kent.ac.uk/15986/> The University of Kent's Academic Repository KAR

The version of record is available from

<https://doi.org/10.1063/1.468427>

This document version

UNSPECIFIED

DOI for this version

Licence for this version

UNSPECIFIED

Additional information

Versions of research works

Versions of Record

If this version is the version of record, it is the same as the published version available on the publisher's web site. Cite as the published version.

Author Accepted Manuscripts

If this document is identified as the Author Accepted Manuscript it is the version after peer review but before type setting, copy editing or publisher branding. Cite as Surname, Initial. (Year) 'Title of article'. To be published in *Title of Journal*, Volume and issue numbers [peer-reviewed accepted version]. Available at: DOI or URL (Accessed: date).

Enquiries

If you have questions about this document contact ResearchSupport@kent.ac.uk. Please include the URL of the record in KAR. If you believe that your, or a third party's rights have been compromised through this document please see our [Take Down policy](https://www.kent.ac.uk/guides/kar-the-kent-academic-repository#policies) (available from <https://www.kent.ac.uk/guides/kar-the-kent-academic-repository#policies>).

The effect of temperature on the structure of amorphous hydrogenated carbon

J. K. Walters, D. M. Fox, T. M. Burke, O. D. Weedon, and R. J. Newport
Physics Laboratory, The University, Canterbury, Kent, CT2 7NR, United Kingdom

W. S. Howells
Neutron Division, Rutherford Appleton Laboratory, Didcot, OX11 0QX, United Kingdom

(Received 24 February 1994; accepted 11 May 1994)

The results of a neutron diffraction study on the structure of amorphous hydrogenated carbon *a*-C:H are presented up to a maximum temperature of 1000 °C. The data show clearly the effect on atomic correlations of elevated temperatures, with the initial room-temperature amorphous network (a mixture of single bonds and olefinic double bonds) becoming progressively aromatic, then graphitic as hydrogen is evolved. Complementary x-ray diffraction and infrared spectroscopy data are also presented, the infrared data enabling a more detailed discussion of the temperature-dependent hydrogen environment, and the x-ray data are used to highlight the change in the carbon network. Comparisons have been made with previous work on similar systems and a brief summary of these results is given.

INTRODUCTION

Over the past 20 years, much work has been carried out on amorphous materials and during this time they have seen continued technological exploitation. As our knowledge of the materials has grown, the number of technological applications and potential applications has also increased. Our understanding of these novel and relatively complex amorphous materials is still far from complete, however, and important questions remain, especially those concerning the atomic-level structure.

A material of contemporary interest is the family of amorphous hydrogenated carbons (*a*-C:H). *a*-C:H may be prepared harder, denser, and more resistant to chemical attack than any other solid hydrocarbon,^{1,2} and these properties, coupled with a high degree of transparency to infrared and histocompatibility have led to many applications.^{3,4} However, *a*-C:H can be produced in a variety of forms, depending on the deposition conditions, ranging from the extremes of the soft polymeric (high hydrogen content and high sp^3 content with many $-CH_2-$ chains) and graphitic (low hydrogen content and high sp^2 content) forms to hard or "diamond-like" *a*-C:H which has mixed bonding and a large degree of cross linking and structural rigidity. The macroscopic properties of the material are then critically dependent on the conditions under which it was prepared,⁵ with the hard forms of *a*-C:H (of central importance to this work) being associated with CVD/PVD processes involving intermediate effective deposition energies and hydrogen contents.

It is self-evident that the bonding in *a*-C:H plays a crucial role in determining the observed properties, particularly the proportion of sp^2 and sp^3 carbon bonding environments. What is required is a structural model for these materials which can be used to relate "bulk" properties to the microscopic or atomic-level structure. Although a full understanding of this relationship does not yet exist, current models incorporate clusters of sp^2 carbon linked via a hydrogenated (or polymeric) sp^3 phase, where it is these interconnections which are said to govern the overall me-

chanical properties of the material. A fuller account can be found in reviews by Angus *et al.*¹ and Robertson.^{2,5-7} Our own diffraction data,^{8,9} together with other experimental and molecular dynamic simulation work,^{10,11} is, however, providing clear evidence of the inadequacies of these models and has provided the basis for an improved model structure.

Attention should be drawn to the important role played by hydrogen in determining the properties of *a*-C:H. As well as the expected chemically bonded hydrogen, trapped molecular hydrogen has been unambiguously detected in small quantities by neutron scattering techniques.¹² Within the Robertson model, hydrogen is seen to stabilize the sp^3 regions, reducing the size of any sp^2 clusters, but at the same time increasing the number of network terminating bonds, leading to a maximum hardness at intermediate hydrogen concentrations.¹

It is well-known that when *a*-C:H is heated, it suffers irreversible hydrogen loss and a structural transformation to graphite (see, e.g., Refs. 13 and 14); it is this process which we wish to study in more detail.

Neutron diffraction has already been found to be an extremely useful technique for the structural investigation of amorphous materials in general^{15,16} and of *a*-C:H, in particular.¹⁷⁻¹⁹ The pulsed neutron source ISIS at the Rutherford Appleton Laboratory (U.K.) allows one to obtain high-resolution real-space data since, unlike electron²⁰ and x-ray¹³ diffraction measurements where the range in k space is very restricted, the ISIS source facilitates a significantly wider dynamic range. Typically, data can be collected between 0.5 and 50 Å⁻¹. The extraction of real-space correlation functions of very high resolution is therefore possible, which in its turn provides an excellent probe for the complex carbon bonding environment associated with *a*-C:H, allowing the sp^2 and sp^3 environments to be distinguished directly.^{8,9} Furthermore, because the neutron, unlike x rays or electrons, scatters from the nucleus, there is no Z -dependent form factor and the correlations involving hydrogen are also accessible. Conversely, this fact may be used to advantage in

TABLE I. Compositional and other information for the sample at different temperatures.

Temperature (°C)	C in sample (±2.0 at. %)	H in sample (±2.0 at. %)	Density (±0.02 g cm ⁻³)	Number density (±0.05 atoms Å ⁻³)
25	65.0	35.0	1.81	0.13
100	63.7	36.3	1.73	0.13
200	63.5	36.5	1.72	0.13
300	66.2	33.8	1.77	0.13
380	65.2	34.8	1.76	0.13
460	71.2	28.8	1.76	0.12
550	80.4	19.6	1.80	0.11
630	85.8	14.2	1.75	0.10
800	93.4	6.6	1.75	0.09
1000	98.7	1.3	1.74	0.09

x-ray diffraction, where it is possible to obtain a pair correlation function which highlights the carbon-carbon correlations only.

Infrared spectroscopy has been used in this study to provide complementary information on the hydrogen bonding environment and the types of hybridization present in *a*-C:H. Previously, Dischler *et al.*²¹ performed an extensive infrared study of the hydrogen bonding environment in *a*-C:H, and he has proposed bonding environment assignments for all observed frequencies. Also, Vandentrop *et al.*²² used infrared spectroscopy to estimate CH₂:CH₃ ratios, but all the infrared results necessarily depend on assumptions for the matrix elements of each vibration and a fully quantitative analysis is very difficult. More quantitatively reliable information on this ratio is obtained from inelastic neutron scattering measurements¹⁸; however, in the work discussed here, we require only qualitative information from the infrared work.

EXPERIMENTAL DETAILS

The *a*-C:H sample used in this series of experiments was prepared using a saddle-field fast-atom (i.e., neutral particle) source^{23,24} with acetylene as the precursor gas. The sample was prepared at an effective beam energy of 500 eV and a system pressure of 1.4×10^{-4} mbar. These deposition conditions pertain to the hard form of the sample Knoop hardnesses of $2000H_k$ have been measured²⁵ for this material (cf. 6000 – $11\,000H_k$ for diamond,¹ although hardnesses greater than $6000H_k$ have also been observed. The sample was prepared in the form of a micron-size powder.

Data were collected for both the neutron diffraction and infrared spectroscopy measurements at a series of temperatures up to 1000 °C, and a combustion analysis was carried out for each temperature using a Carlo-Erba CHN combustion analyzer. Also an "initial" density was evaluated using a residual volume technique and then, using this baseline value and the results of the combustion analysis, the number densities for the heat-treated samples were determined. The results of all these measurements are summarized in Table I. The neutron diffraction data were collected from a single sample which was heated *in situ* in a vacuum furnace. The infrared data derive from samples (from the same batch), which were preheated for 4 h under vacuum.

Diffraction studies

The neutron diffraction work presented here was carried out at the pulsed neutron facility ISIS at the Rutherford Appleton Laboratory (UK) on the instrument LAD,²⁶ which is particularly well-suited for the study of covalently bonded amorphous materials due to the wide dynamic range available (up to 50 \AA^{-1}). The ISIS spallation source produces neutrons with a spread of velocities, and therefore a spread of arrival times at any detector, giving a smooth variation in neutron wavelength as a function of time of flight (TOF). Neutrons are scattered from the sample into fixed angle detectors on each side of the instrument, and for each detector pair (i.e., at a given scattering angle 2θ), the scattered neutron intensity is measured as a function of TOF, which can itself be directly related to momentum transfer. The complete scattering profile is then obtained by combining overlapping spectra from several detector angles. Also, monitors in the incident and transmitted beam record TOF spectra to provide information on the total neutron cross section and the intensity:wavelength profile of the incident beam. Each experiment requires measurements for the sample, the empty sample container, a background in the absence of sample, and a vanadium rod with a geometry comparable to the sample and its container. The vanadium rod measurement supplies the information necessary to put the sample scattering on an absolute scale since it has an almost entirely incoherent neutron cross section which is well known.²⁷ A schematic representation of the scattering arrangement is shown in Fig. 1.

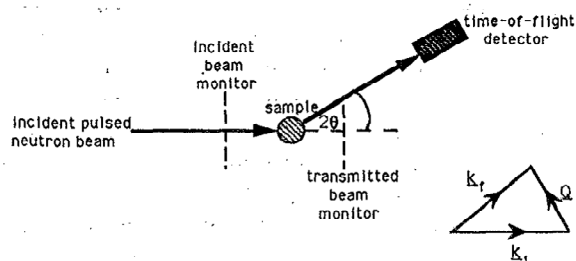


FIG. 1. A schematic representation of the neutron experimental arrangement.

In performing a diffraction experiment, the quantity we wish to obtain is the structure factor $S(Q)$, where for an amorphous material (i.e., an isotropic scatterer)²⁷

$$S(Q) = 1 + \frac{4\pi\rho}{Q} \int_0^\infty r dr [g(r) - 1] \sin(Qr), \quad (1)$$

where ρ is the average number density of atoms in the material, $|Q_-| = |k_{i-} - k_{f-}|$ is the wave vector transfer associated with the diffraction experiment, which for elastic scattering from a liquid or amorphous solid is defined as $Q = (4\pi/\lambda)\sin\theta$, where 2θ is the scattering angle and λ is the neutron wavelength, and $g(r)$ is the pair correlation function, which is a measure of the atomic density at a distance r from a given atom at the origin. The pair correlation function may be obtained by Fourier transformation of the structure factor, which is directly related to the measured neutron scattering intensity.

In a multicomponent system, there are contributions to the total structure factor from each atom-type pair. For a binary system such as *a*-C:H, we therefore have three independent contributions which are weighted to give the total structure factor. The corresponding function in real space is the total pair distribution function $G(r)$, which is a weighted combination of partial pair distribution functions (according to the Faber-Ziman formalism²⁷)

$$G(r) = \sum_\alpha \beta [c_\alpha c_\beta b_\alpha b_\beta g_{\alpha\beta}(r)], \quad (2)$$

where c_α is the atomic fraction and b_α is the coherent scattering length, respectively, of element α , and where $g_{\alpha\beta}(r)$ represents the partial terms in $G(r)$ and describes the probability of finding an atom of type β at a distance r from an atom of type α at the origin. From the weightings of the partial terms, it is evident that the dominant terms will be those arising from the carbon-carbon and carbon-hydrogen correlations, with the carbon-hydrogen correlations appearing as troughs rather than peaks since b_H is negative (due to the π phase shift experienced by a neutron on scattering from hydrogen; the correlation must also be equivalent to the hydrogen-carbon correlation term).

The derivation of these equations is predicted on the validity of the static approximation^{28,29} which requires that any change in a neutron's energy upon scattering is small compared to its incident energy. Before the structure factor can be generated, several corrections have to be made to the raw data,³⁰ the major ones being for background, container and multiple scattering, attenuation, and the effects of inelasticity. By far the most problematic of these is the inelasticity correction for deviations from the static approximation. Analytic approaches such as Refs. 31-33 break down for low mass atoms, especially hydrogen, and so an empirical method has been adopted. This involves fitting a low order polynomial through the data to remove the underlying self-scattering curve; to first order, the effects on inelastic scattering are embedded in this term. There are problems with applying this method, particularly concerning the subsequent quality of the data at very low r values (below $\sim 1\text{\AA}$) and

particularly for hydrogen correlations at short distances; this fact must be borne in mind when conclusions are drawn from the $G(r)$.

Also, as will be seen in the data, the effective Q range of the structure factor for the elevated temperature experiments only extends down to $\sim 3\text{\AA}^{-1}$. This is due to a problem with the furnace scattering at low scattering angles. However, the absence of these low Q data in the $S(Q)$ data does not affect the conclusions drawn from the results.

Analogous statements may be made about the analysis of x-ray diffraction data, although in this case, the weighting coefficients in the $G(r)$ include a form factor, which is dependent on the atomic number Z . It is apparent then that the pair correlation function determined in this way will approximate to the partial $g_{cc}(r)$. The x-ray data shown here, which are part of an extensive series of synchrotron x-ray diffraction studies on *a*-C:H to be published elsewhere, may therefore be used to isolate the changes occurring in the underlying carbon network from the overall picture provided by neutron diffraction. It also provides something of a consistency check on the data analysis procedures.

The x-ray structure factor for the sample that had been heated to 1000 °C as part of the neutron experiment was determined by standard $\theta:2\theta$ x-ray diffraction using station 9.1 at the Daresbury Laboratory synchrotron radiation source, Warrington (UK). The raw data are first corrected for any background, polarization, and scattering volume effects, then the self-term and Compton scattering contributions are removed by fitting and subtracting a polynomial. The resultant interference function is finally corrected for absorption. Any misalignment of the Compton contributions resulting from this empirical correction may have some residual effect on the relative peak heights in the structure factor, but accurate interatomic distances can still be extracted from the data.

Infrared spectroscopy

Infrared spectroscopy is particularly well suited as a probe of the bonded hydrogen. In this experiment, infrared characterization measurements were performed using a Bio Rad Diffuse Reflectance Infrared Fourier Transform (DRIFT) FTS60 spectrometer.

Given the intrinsic difficulties associated with any attempt to analyze infrared data quantitatively, we here concentrate on using Gaussian peak fits to the fundamental carbon-hydrogen stretch modes to examine the overall nature of the hydrogen bonding environment, and its qualitative variation between samples preheated to the temperatures shown in Table I.

RESULTS AND DISCUSSIONS

Combustion analysis

From the results of the combustion analysis, it is possible to look at the variation of hydrogen content in the sample as a function of temperature (see Fig. 2). It is clear that hydrogen evolution is a continuous process, with irreversible changes occurring even by 300 °C, but with a rapid increase in the rate of hydrogen evolution thereafter. These data should be compared with the calorimetry work of

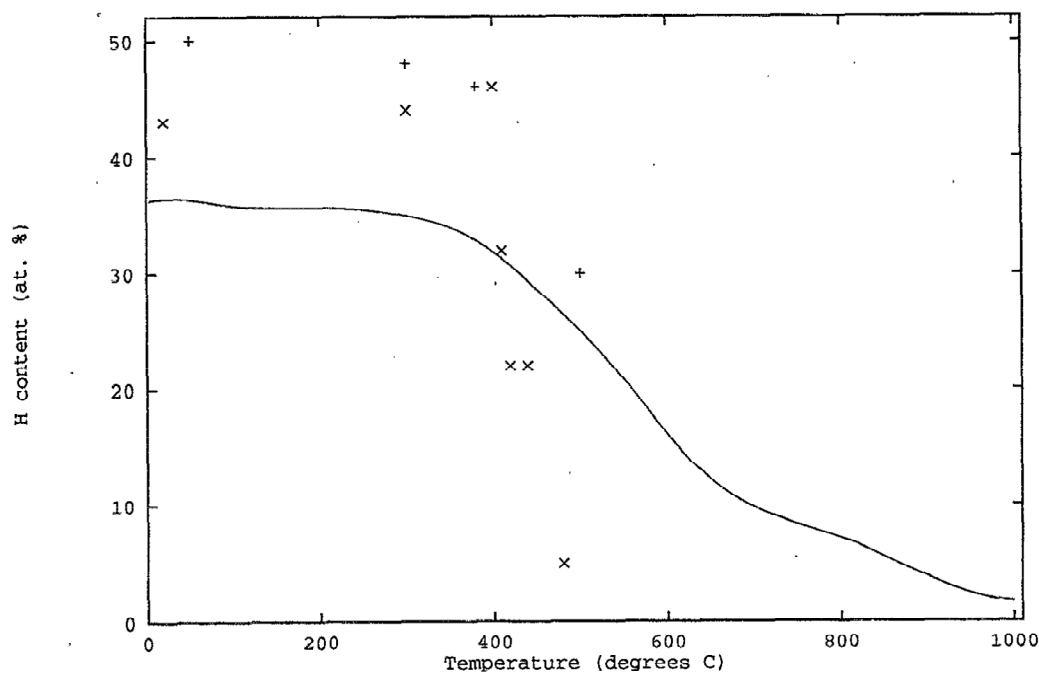


FIG. 2. Hydrogen content of the sample as a function of temperature (solid line) compared to the data of Lukins (Ref. 34) (+) and Yasuda (Ref. 35) (×) (for this data only the y scale is arbitrary).

Nyaiesh and Nowak³⁶ on similar materials, which suggested the presence of significant exothermic transitions at ~ 550 and ~ 750 °C. Our own calorimetry measurements failed to identify any transition temperature, but the combustion analysis results would seem to indicate that a “threshold” temperature in the region of 300 °C does exist. We have no such supportive evidence for a threshold/transition at higher temperatures. It is important to note, however, that their sample was deposited in a markedly different way to ours (glow discharge using a methane precursor), and their experiments carried out on a sample prepared in such a way as to maximize its surface area—and hence enhance the effective sensitivity of the measurement.³⁷

Table II compares threshold temperatures and maximum hydrogen effusion rates for various samples as compared to the hydrogen content of the as-prepared sample. We note that

the general trend is that for samples with an initially high hydrogen content, effusion begins at a lower temperature than for those where the prepared sample has a low hydrogen content, i.e., as the initial hydrogen content increases, the threshold temperature for hydrogen effusion decreases. The temperature at which the effusion rate reaches as maximum is generally in the range 450–600 °C, irrespective of hydrogen content.

Neutron and x-ray diffraction

Figures 3 and 4 show the structure factors and pair correlation functions, respectively, for each of the temperatures derived from neutron diffraction spectra, and for the analogous 1000 °C x-ray spectrum. From each pair distribution function, a radial distribution function $J(r)$ can be generated

TABLE II. “Threshold” temperatures and temperatures for maximum rates of hydrogen evolution for various samples.

Sample	As-prepared hydrogen content	Temperature at which hydrogen evolution begins (°C)	Temperature for maximum rate of hydrogen evolution (°C)
Gonzalez-Hernandez ^a	Low	~ 600	...
Gonzalez-Hernandez ^a	Medium/high	~ 400	~ 500
Nyaiesh <i>et al.</i> ^b	~ 25 at. %	~ 450	~ 550
Our sample	~ 35 at. %	~ 300	~ 500
Dischler ^c	~ 39 at. %	~ 300	~ 550
Lukins ^d	~ 50 at. %	~ 300	~ 500

^aReference 38.

^bReference 36.

^cReference 21.

^dReference 34.

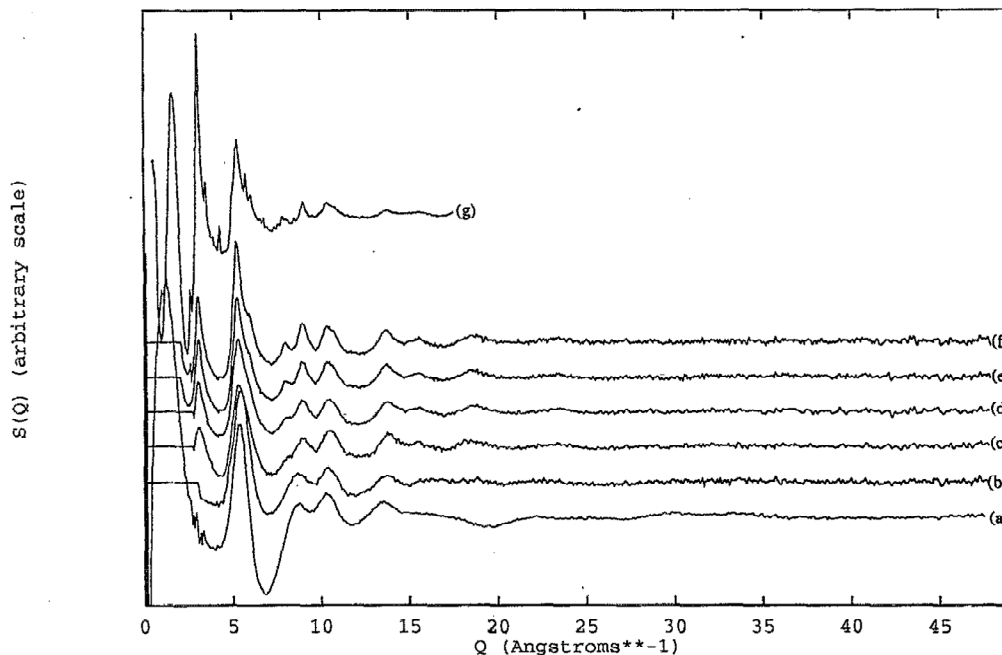


FIG. 3. The structure factor $S(Q)$ at (a) 25; (b) 300; (c) 550; (d) 630; (e) 800; and (f) 1000 °C derived from neutron data; and (g) at 1000 °C from x-ray data.

where $J(r) = 4\pi r^2 \rho G(r)$ and provides a direct count of the number of atomic centers at a distance r from the origin. From this function, an indication of the carbon-carbon coordination number can be obtained by fitting the first shell peak with a series of Gaussians allowing both position and area to vary, and therefore the change in the carbon-carbon

coordination number as the temperature is increased can be investigated (see Fig. 5). Also, the positions of the peaks in the $J(r)$ give an indication of the change in average bond length, which for the carbon-carbon first coordination shell, in particular, shows clearly the change in the type of bonding (see Table III).

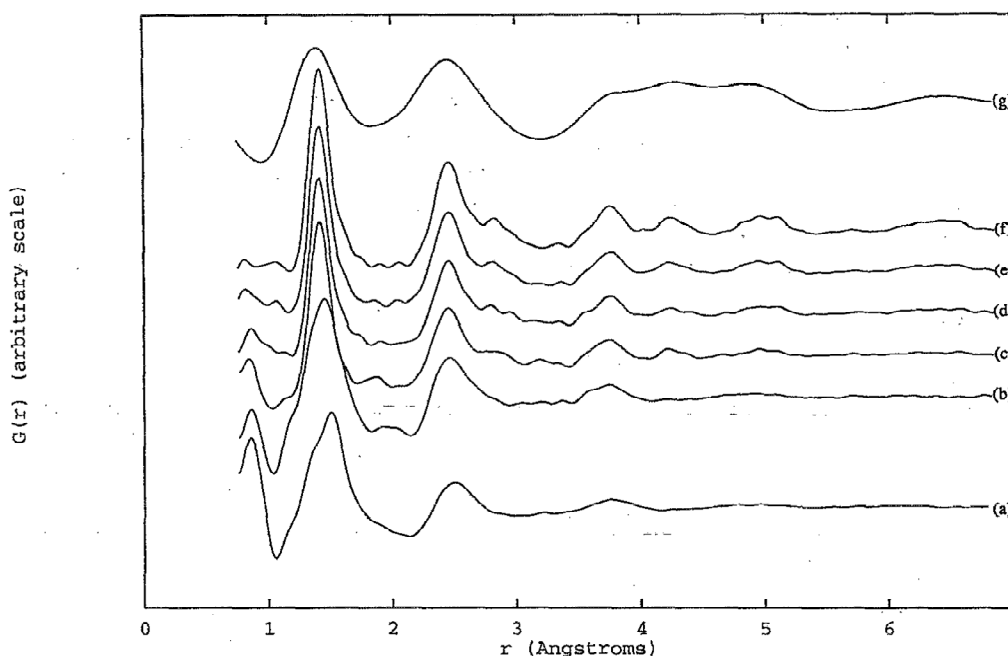


FIG. 4. The total distribution function $G(r)$ at (a) 25; (b) 300; (c) 550; (d) 630; (e) 800; (f) 1000 °C derived from neutron data; and (g) at 1000 °C from x-ray data.

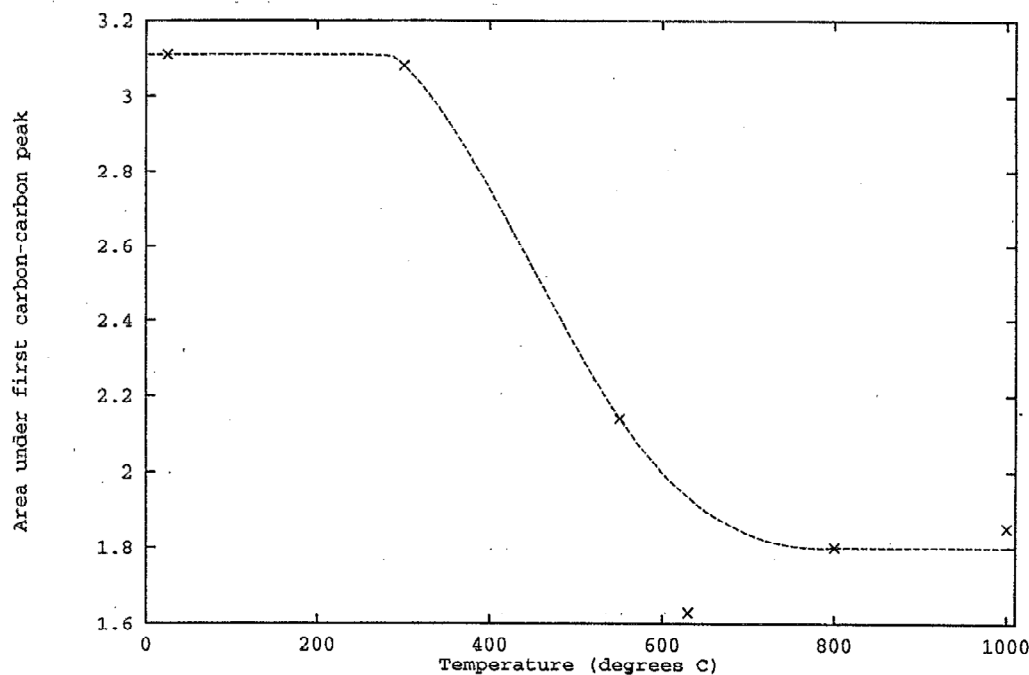


FIG. 5. The area under the carbon-carbon first neighbor peak (± 0.3) as a function of temperature.

From Fig. 4, it is clear that as the temperature is increased, the carbon-carbon peak moves from a broad peak at ~ 1.5 Å [although from the slight asymmetry of the peak, we can postulate that in fact it has two components — a peak at ~ 1.3 Å corresponding to sp^2 (olefinic) carbon-carbon and a peak at ~ 1.54 Å corresponding to the sp^3 carbon-carbon, as has been observed in other, more detailed measurements at room temperature⁸] to a narrow peak centered at ~ 1.4 Å; a change is already apparent at 500 °C. There is therefore a definite trend for the carbon-carbon bonding environment to move from sp^3 to sp^2 and for the olefinic sp^2 to become more aromatic/graphitic in character. Further evidence for this can be found in the decrease in the area under the first-shell carbon-carbon peak shown in Fig. 5.

Also, although the quality of the low r data is subject to larger uncertainty due to the empirical nature of the inelasticity correction, there is clearly a gradual weakening of the

carbon-hydrogen trough at ~ 1.0 Å and the hydrogen-hydrogen peak at ~ 0.8 Å, as would be expected given that, as the temperature is increased and hydrogen is evolved, the number of carbon-hydrogen bonds and the amount of molecular hydrogen present is reduced. Finally, the second-shell carbon-carbon-carbon correlations giving rise to the peak at ~ 2.5 Å should be highlighted. This peak is seen to sharpen as the temperature is increased, which indicates a move from a mixed towards a single carbon bonding environment. The second shell peak position at 1000 °C is consistent with a second neighbor separation of 2.47 Å, which implies an average bond angle of 120° (i.e., as would be expected from π -bonded graphite).

It is apparent from the x-ray data shown in Figs. 3 and 4 that our conclusions concerning the changes in carbon-carbon network bonding are borne out, with the position of the (less well-resolved) first shell peak being 1.42 Å, and a final second shell peak position consistent with graphitic bond angles.

Although the maximum Q value of the x-ray data is less than that for the equivalent TOF neutron data and hence provides poorer real-space resolution, the k -space, x-ray data are actually more clearly resolved. Bragg peaks resulting from the formation of graphite crystallites are clearly visible in these data.

Infrared spectroscopy

The infrared spectra for each of the annealing temperatures are shown in Fig. 6. For each temperature, the absorbance peaks in the C-H stretch region, (3400 – 2600 cm^{-1}) were fitted with a series of Gaussians [see Figs. 7(a)–7(g)] with the frequency position fixed and the width and height

TABLE III. Bond distances and their assignments at the different temperatures.

Temperature (°C)	Position of the first C-C shell ± 0.01 (Å)	Assignment
25	1.34	C=C olefinic
	1.52	C-C
	1.38	C=C
300		olefinic/graphitic and/or aromatic
	1.51	C-C
550	1.42	C=C graphitic
630	1.41	C=C graphitic
800	1.42	C=C graphitic
1000	1.42	C=C graphitic

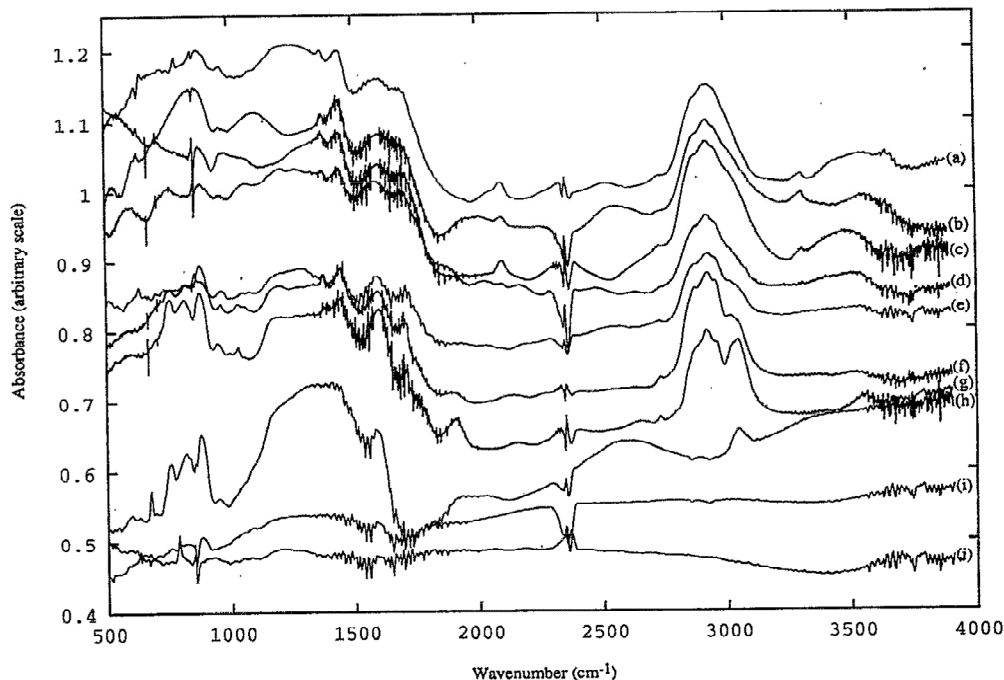


FIG. 6. Infrared spectra at (a) 25; (b) 100; (c) 200; (d) 240; (e) 300; (f) 380; (g) 460; (h) 550; (i) 630; and (j) 800 °C.

allowed to vary; Table IV summarizes the results for each of the temperatures, together with the vibrational assignments. By its very nature, infrared data cannot be fully quantitative, but still allow broad conclusions to be drawn on the concentrations of the various structural units observed. A comparison with Dischler's result would indicate that our data is of slightly lower resolution; however, the Gaussian fits obtained are satisfactory as a means of providing qualitative information on the trends occurring. In order to allow a comparison between the samples annealed at different temperatures, the peak areas given in Table IV have all been normalized so that the total area in the range 2600–3400 cm^{-1} correlates with the decreasing hydrogen content of the samples. The general decrease in linewidth of the $\sim 3000 \text{ cm}^{-1}$ peak with increasing temperature is associated with a reduction in the variety of sp^2 CH (olefinic/aromatic) hydrogen bonding environments.

We can see that the trends observed are similar to those seen by Dischler,²¹ Yasuda,³⁵ and Lukins,³⁴ where the increasing aromatic character with temperature is seen in the appearance of the sp^2 CH (aromatic) stretch around 3050 cm^{-1} , together with a corresponding decrease in magnitude of the sp^2 CH (olefinic) stretch (3000 cm^{-1}), and peaks associated with sp^3 CH₂ and CH₃ symmetric and antisymmetric stretches (2870, 2920, and 2690 cm^{-1}). One other point of note is that the infrared measurements detect the presence of sp^1 CH, which neutron diffraction cannot do without ambiguity (since the strongly negative carbon–hydrogen correlation will obscure a weak sp^1 carbon–carbon correlation). X-ray data has too poor a real-space resolution to distinguish the various carbon–carbon bond lengths.

At room temperature, we observe in our sample the same

features as seen by Dischler and Yasuda, except that, like Lukins, we see that our sample does contain some CH₃ groups (although quantitative inelastic neutron scattering data on the same samples shows that such groups are present in small concentrations only¹²). As the temperature is increased to 240 °C, we can see, looking at the normalized peak areas in Table IV, that while there has been only a small loss of hydrogen, some structural changes have already occurred. The areas for both the sp^3 CH₂ and CH₃ symmetric ($\sim 2860 \text{ cm}^{-1}$) and the sp^3 CH₃ antisymmetric ($\sim 2960 \text{ cm}^{-1}$) stretches have reached their maximum values. However, at the same time, the area of the sp^3 CH₂ antisymmetric ($\sim 2920 \text{ cm}^{-1}$) peak is at a minimum. So there is a definite movement of hydrogen within the network which results in the formation of CH₃ network-terminating groups, at the expense of CH₂ groups. Further evidence for this hydrogen transport comes from the increase in area of the sp^2 CH (olefinic) stretch peak ($\sim 3000 \text{ cm}^{-1}$) between room temperature and 200 °C. As hydrogen is lost from CH₂ groups, it is transported through the network via the formation of olefinic C–H bonds to CH₃ groups. This would appear to be the first stage in structural rearrangement that appears to occur before significant hydrogen evolution has begun. Following this, there is then a reorganization of the carbon network. Between 300 and 460 °C, we observe that the sp^2 CH (olefinic) stretch peak ($\sim 3000 \text{ cm}^{-1}$) moves to a position of $\sim 3050 \text{ cm}^{-1}$, which may be assigned to sp^2 CH (aromatic) stretching. In Dischler's and Yasuda's data, we see a similar transformation with the gradual loss of the olefinic CH stretch and growth of the aromatic CH stretch peaks. From our data, which are of lower resolution, it is only possible to say that the peak around 3000 cm^{-1} is a combination of the

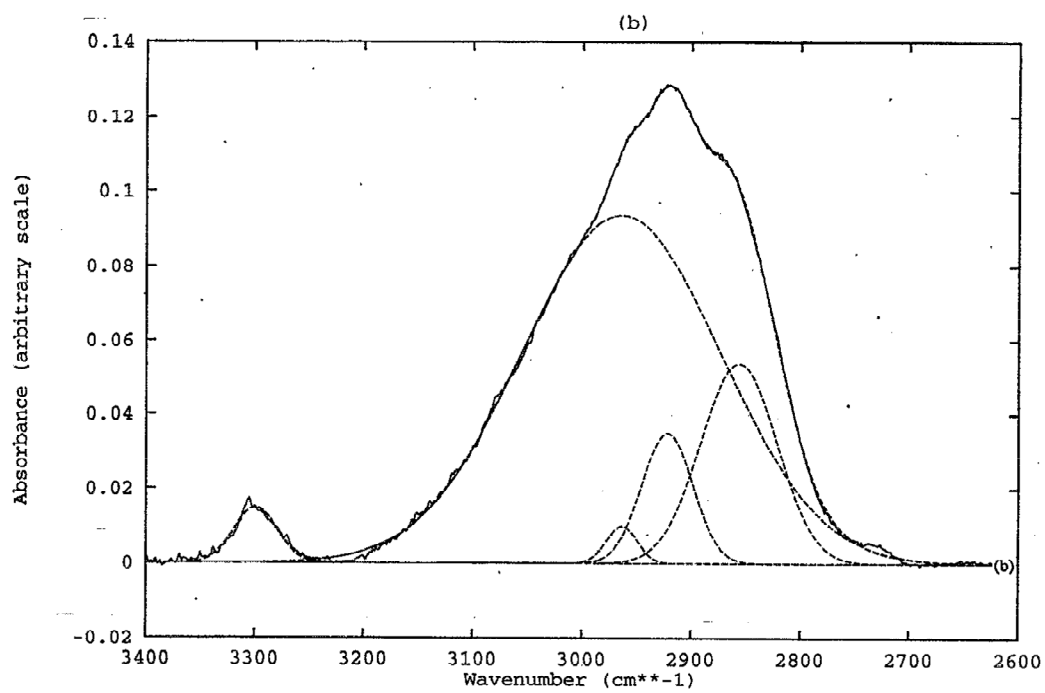
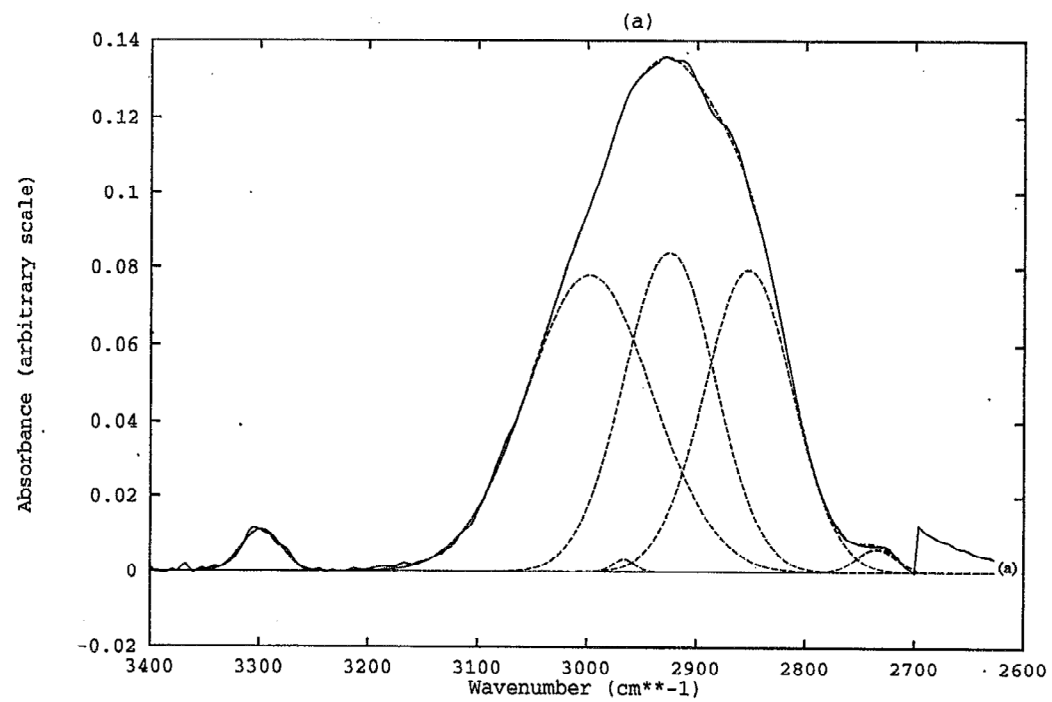


FIG. 7. (a)–(f) Infrared data (solid line) with the fitted Gaussians (broken lines) for temperatures between 25 and 460 °C.

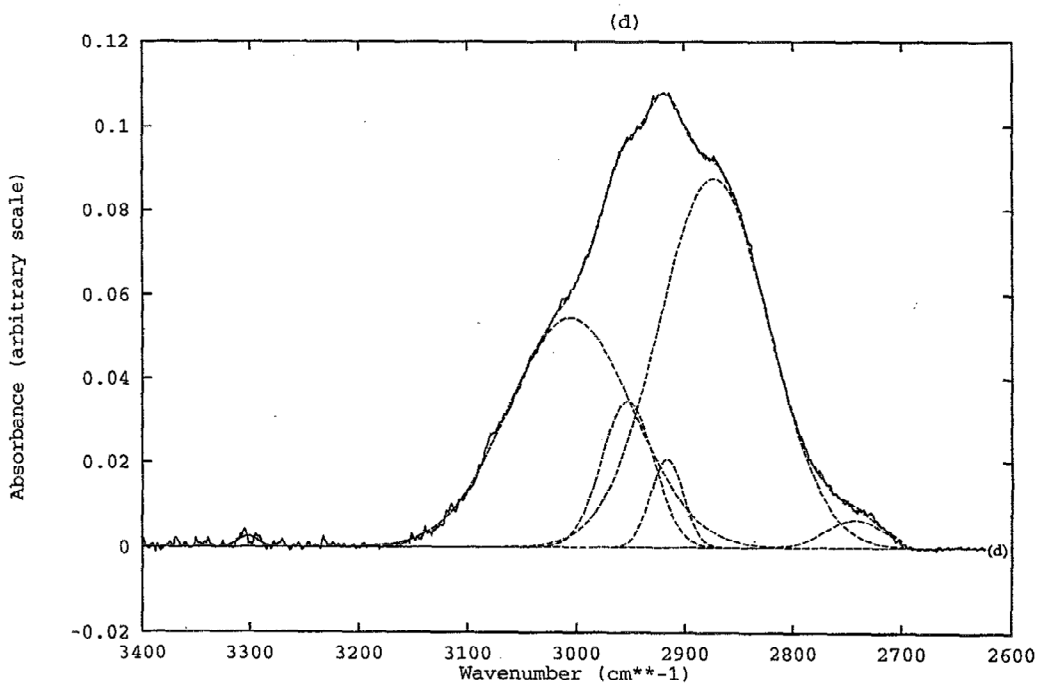
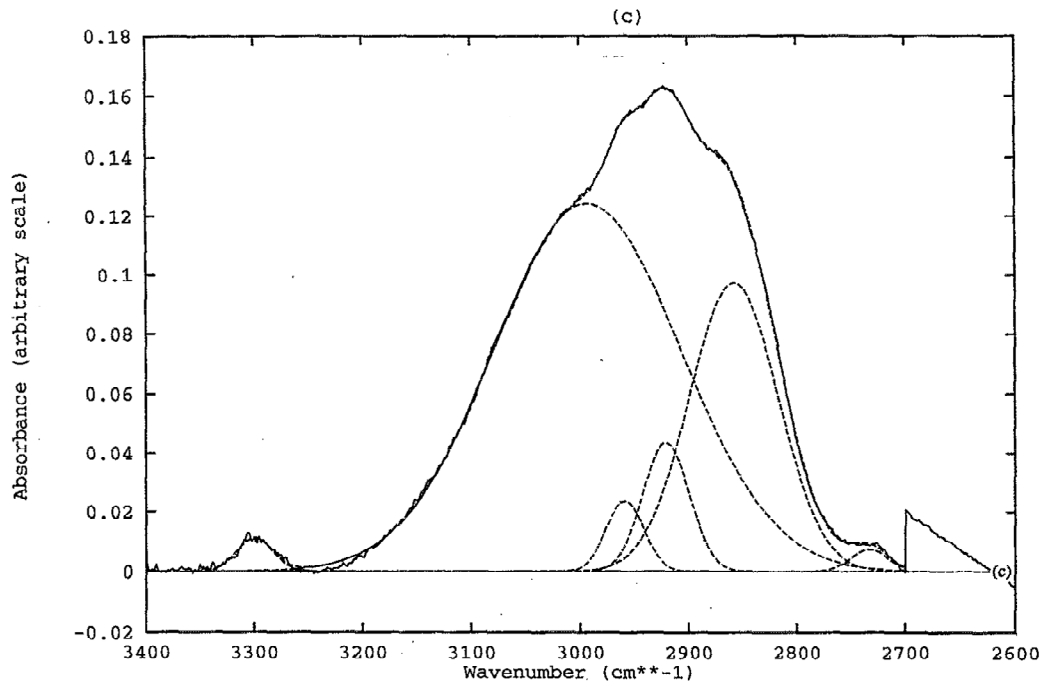


FIG. 7. (Continued.)

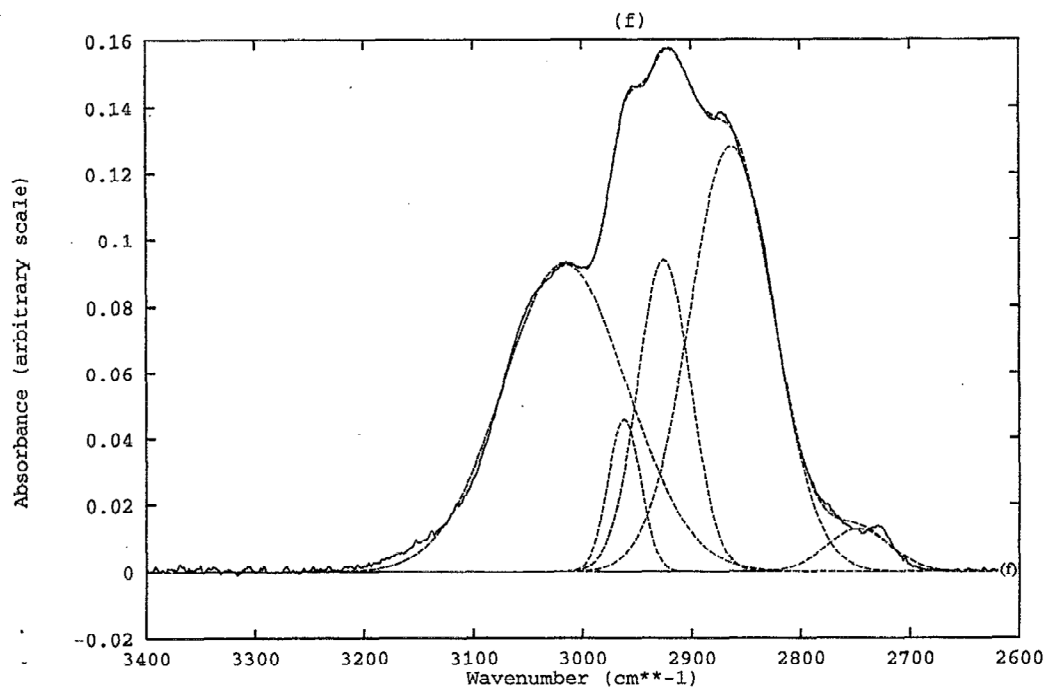
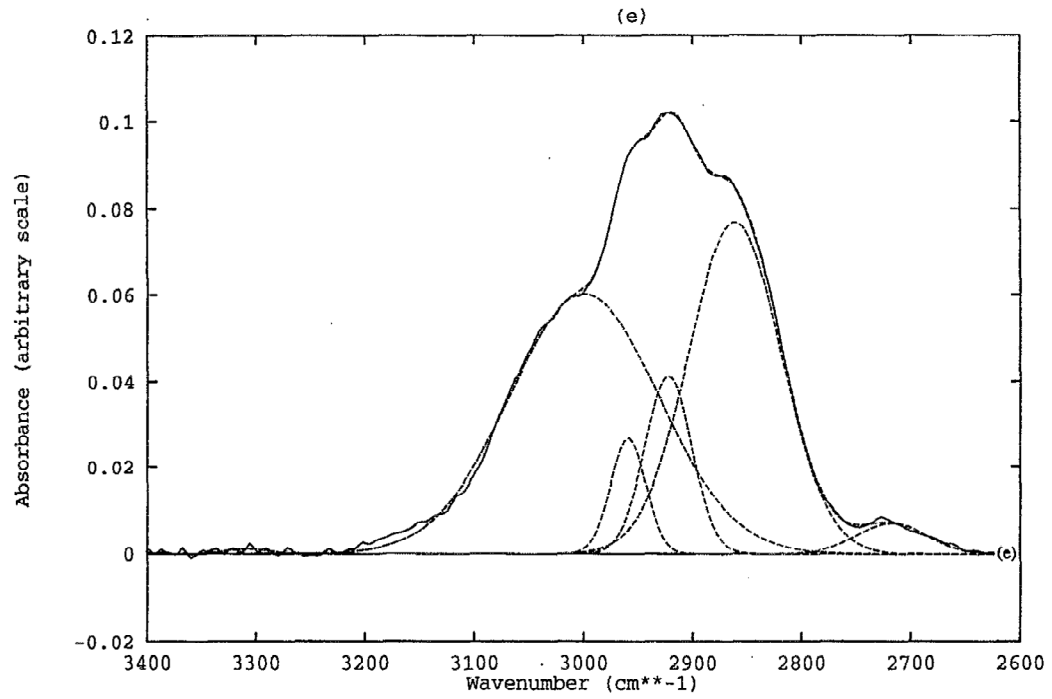


FIG. 7. (Continued.)

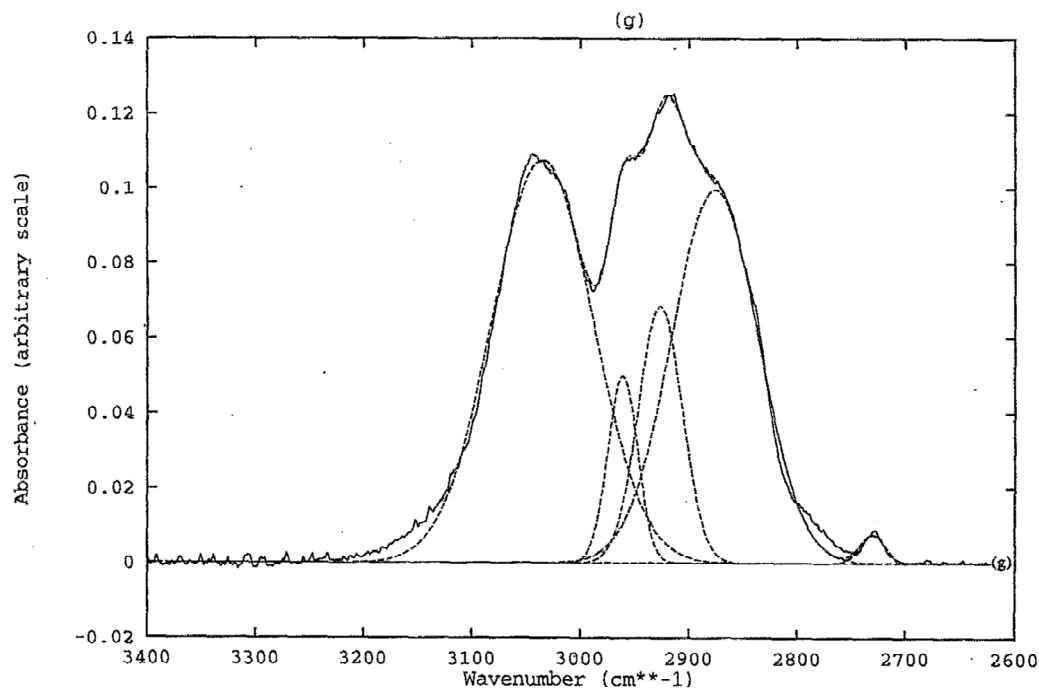


FIG. 7. (Continued.)

olefinic sp^2 CH (~ 3000 cm^{-1}) and the aromatic sp^2 CH (~ 3035 cm^{-1}). With increasing temperature, the olefinic peak lessens and the aromatic peak grows, and this manifests itself as a drift in peak position from 3000 to 3035 cm^{-1} . So even before significant loss of hydrogen has occurred, the network has a highly aromatic character. On heating above 460 °C, all the peaks are seen to decrease (see Fig. 7) as hydrogen is rapidly evolved. Also, note that as the sample is heated, the area of the peak at 3300 cm^{-1} (sp^1 CH stretch) decreases, so that at 460 °C, no sp^1 CH remains.

From Fig. 7, we can also note the presence of various CH bending vibrations for CH_2 and CH_3 at 740, 835, 1050, 1080, 1375, and 1450 cm^{-1} . Since in this region the spectra are relatively noisy, the changes with temperature are not examined in detail, although they are consistent with those described by the CH stretch region.

Our results show quite clearly the general trend from sp^3 to sp^2 bonding. Proposed mechanisms for the structural changes given by Refs. 21, 39, and 40 in conjunction with our own findings would seem to indicate that sp^3 CH is the primary source of hydrogen for effusion, such that, on annealing, molecular hydrogen is formed wherever there are two neighboring hydrogen atoms. Only on annealing to relatively high temperatures is hydrogen lost from any remaining sp^2 CH, and graphitization is complete.

CONCLUSIONS

From the evidence, it appears that there are two stages to the hydrogen evolution process: up to 300 °C, very little hydrogen is evolved, but from the neutron diffraction and infrared results, significant structural reorganization does occur

TABLE IV. Observed frequencies and normalized areas from the infrared data with their assignments.

Assignment	Observed frequency (cm^{-1})	Normalized peak area at 25 °C	Normalized peak area at 100 °C	Normalized peak area at 200 °C	Normalized peak area at 240 °C	Normalized peak area at 300 °C	Normalized peak area at 380 °C	Normalized peak area at 460 °C
sp^1 CH	3298–3308	0.69	1.1	0.48	0.11	0.09	0.01	0.00
sp^2 CH (olefinic/aromatic)	2966–3035	16	30	28	14	18	16	15
sp^3 CH_3 (asymmetry)	2953–2966	0.12	1.1	1.1	3.9	1.9	2.0	2.1
sp^3 CH_2 (asymmetry) and sp^3 CH	2917–2927	12	2.1	2.4	1.5	3.9	6.9	4.2
sp^3 CH_3 and CH_2 (symmetry)	2850–2880	11	7.5	10	20	15	15	12

TABLE V. A summary from the literature of the effects of annealing on a variety of samples.

Reference	Composition	Preparation	Characteristics of the as-prepared sample	Characteristics of heat treated sample
Lukins (Ref. 34)	50% C 50% H	D.c. magnetron glow discharge C_2H_2 -Ar	Small, significantly substituted aromatic groups. Nonaromatic C as a highly connective network. Tetrahedral network	70% C 30% H Aromaticity ~ 1.0 Aromatic clusters—possible olefinic linking.
Craig (Ref. 39)	50.7% C 42.6% H 6.7% O	D.c. magnetron sputtering C_2H_2 -Ar	modified by C=C bonds. Crystallite size < 6 Å. Some five-, six-, and seven-fold rings.	66.1% C 31.9% H 1.9% O Increased amount of sp^2 bonding. 66% C 32% H 2% O Defective graphite planes—possible tetrahedral linking.
McKenzie (Ref. 41)	51% C 43% H 7% O	D.c. magnetron glow discharge C_2H_2 -Ar	sp^3 C dominates with some aromatic C. Much CH_3 , some CH_2 , some C=C.	Highly microporous throughout. Porosity ~ 0.40 .
Yin (Ref. 42)		D.c. magnetron glow discharge C_2H_2 -Ar	Mesoporous; porosity ~ 0.15 . $\sim 75\%$ polymeric. $\sim 14\%$ diamond-like. $\sim 11\%$ graphitic.	$\sim 82\%$ graphitic.
Smith (Ref. 43)		Rf couple glow discharge (low rf power) CH_4	Polymeric. CH_3 dominant. High H content.	Microcrystalline graphite. Condensed ring structure. Long range order.
Gonzalez-Hernandez (Ref. 38)		Rf couple glow discharge (high rf power) CH_4	More graphitic, less polymeric. CH_2 dominant. Low H content.	Microcrystalline graphite. Condensed ring structure. Long range order.
Gonzalez-Hernandez (Ref. 38)		Plasma deposition CH_4		
Couderc (Ref. 40)		(high pressure) Rf glow discharge CH_4	sp^2 C-H dominant. High H content. Polymeric component. $\sim 19\%$ bonded H; $\sim 6\%$ chemisorbed H. Distorted graphite structure.	Increased sp^2 C content. More graphitic.
Nyaiesh (Ref. 36)	$\sim 75\%$ C $\sim 25\%$ H	D.c. PCV deposition CH_4 -Ar		Microcrystalline. Graphitic.
Kumar (Ref. 44)	$\sim 100\%$ C	Rf plasma deposition benzene	Predominant sp^3 C bonding. DLC.	Dominant trigonal (sp^2) crystallites. Graphitic.
Dischler (Ref. 21)	61% C 39% H	Ion beam deposition	sp^3 C: sp^2 C = 2/3:1/3. CH dominant over CH_2 .	$\sim 0\%$ sp^3 C. sp^3 C. sp^2 C = 0:1. Completely aromatized.
This work	65% C 35% H	deposition C_2H_2	sp^3 C-C bonds: sp^2 C-C bonds $\sim 2.6:1$.	sp^3 C-C bonds: sp^2 C-C bonds = 0:1. C-C bond distance ~ 1.42 Å. Aromatized.

in this temperature region. Above 300 °C, hydrogen evolution begins to occur at a much higher rate such that, by 800 °C, over 75% of the total hydrogen within the sample has been lost. By the same temperature, the process of graphitization is well advanced (evident from the trends seen in both the neutron and infrared data, i.e., the move from sp^3 to sp^2 bonding). It should be emphasized that structural transformations are seen to occur throughout the heating process, i.e., there is limited evidence for “transition temperatures” at which dramatic changes occur. This is in contrast to the differential scanning calorimetry experiments carried out by Nyaiesh and Nowak³⁶ who found well-defined transitions occurring in their (somewhat different) sample when it was heated.

A summary of the characteristics of samples before and after annealing is given in Table V. Whatever the nature of the as-prepared sample there is always an increase in sp^2 C

bonding on annealing. The annealed sample is therefore primarily graphitic or aromatic depending on the amount of hydrogen remaining following heat treatment. In some cases, where the initial hydrogen content of the sample was low and the highest temperature reached in the annealing process was relatively high, microcrystalline graphite was observed. Therefore we have a transition from the as-prepared sample to an aromatic ring structure, then to a disordered graphitic ring structure, and finally to microcrystalline graphite.

It would be interesting to look at these structural changes in more detail using neutron diffraction and inelastic neutron scattering, especially between room temperature and 400 °C. Work is already planned to obtain more reliable low r information from steady-state (reactor) neutron diffraction experiments, which will enable a more detailed examination of the hydrogen environment.

On the mesoscopic scale, it is of interest to use small

angle x-ray scattering (SAXS) to study the effects of temperature on the pore structure. McKenzie⁴¹ and Yin⁴² have noted in their samples an initial increase in pore size followed by a collapse of the porous structure, and SAXS will provide the analogous information for our samples; these experiments are already planned and the results will be presented in due course.

ACKNOWLEDGMENTS

We would like to thank Mr. A. Fassam and Mr. G. Bradley (Chemistry Department UKC), respectively, for their help in the combustion analysis and infrared experiments, and also Dr. D. W. Huxley and Mr. D. T. Bowron for their help in the data analysis. We are grateful to Dr. P. J. R. Honeybone for useful discussions. JKW and TMB acknowledge the receipt of SERC studentships.

- ¹J. C. Angus, P. Koidl, and S. Domitz, in *Plasma Deposited Thin Films*, edited by J. Mort and F. Jansen (CRC, Boca Raton, FL, 1986).
- ²J. Robertson, *Adv. Phys.* **35**, 317 (1986).
- ³A. H. Lettington, in *Diamond and Diamond-like Films and Coatings*, edited by R. E. Clausing, L. L. Horton, J. C. Angus, and P. Koidl (Plenum, New York, 1991).
- ⁴J. Franks, K. Enke, and A. Richardt, *Metals and Materials* (1990).
- ⁵J. Robertson, *Prog. Solid State Chem.* **21**, 199 (1991).
- ⁶J. Robertson, *Diamond Relat. Mater.* **1**, 397 (1992).
- ⁷J. Robertson, *Phys. Rev. Lett.* **68**, 220 (1992).
- ⁸J. K. Walters, P. J. R. Honeybone, D. W. Huxley, R. J. Newport, and W. S. Howells, *J. Phys. Condensed Matter* **5**, L387 (1993).
- ⁹J. K. Walters, P. J. R. Honeybone, D. W. Huxley, R. J. Newport, and W. S. Howells, *Phys. Rev. B* (to be published).
- ¹⁰T. Frauenheim, P. Blaudeck, U. Stephan, and G. Jungnickel, *Solid State Commun.* **85**, 997 (1993).
- ¹¹G. Jungnickel, T. Frauenheim, P. Blaudeck, U. Stephan, and R. J. Newport, *Phys. Rev. B* (to be published).
- ¹²P. J. R. Honeybone, R. J. Newport, W. S. Howells, J. Tomkinson, S. M. Bennington, and P. J. Revell, *Chem. Phys. Lett.* **180**, 145 (1991).
- ¹³J. Fink, T. Muller-Heinzerling, and J. Pfluger, *Solid State Commun.* **47**, 687 (1983).
- ¹⁴D. A. Anderson, *Philos. Mag.* **35**, 17 (1977).
- ¹⁵G. Etherington, A. C. Wright, J. T. Wenzel, J. C. Dore, J. H. Clarke, and R. N. Sinclair, *J. Non-Cryst. Solids* **48**, 265 (1982).
- ¹⁶P. A. V. Johnson, A. C. Wright, and R. N. Sinclair, *J. Non-Cryst. Solids* **58**, 109 (1983).
- ¹⁷P. J. R. Honeybone, R. J. Newport, W. S. Howells, and J. Franks, *Diamond and Diamond-like Films and Coatings*, edited by R. E. Clausing *et al.* (Plenum, New York, 1991).
- ¹⁸P. J. R. Honeybone, R. J. Newport, W. S. Howells, and J. Franks, *Diamond Relat. Mater.* **1**, 293 (1992).
- ¹⁹P. H. Gaskell, A. Saeed, P. Chieux, and D. R. McKenzie, *Philos. Mag. B* **66**, 155 (1992).
- ²⁰D. R. McKenzie, L. C. Botton, and R. C. McPhedran, *Phys. Rev. Lett.* **51**, 280 (1983).
- ²¹B. Dischler, A. Bubenzer, and P. Koidl, *Solid State Commun.* **45**, 105 (1983).
- ²²G. J. Vandentrop, M. Kawasaki, K. Kobayashi, and G. A. Somorjai, *J. Vac. Sci. Technol. A* **9**, 1157 (1991).
- ²³J. Franks, *J. Vac. Sci. Technol. A* **7**, 2307 (1989).
- ²⁴J. Franks, *Vacuum* **34**, 259 (1984).
- ²⁵A. Dehbi-Alaoui, A. Matthews, and J. Franks, *Surf. Coatings Technol.* **47**, 722 (1991).
- ²⁶Report RAL-90-041.
- ²⁷R. J. Newport, in *Neutron Scattering at a Pulsed Source*, edited by R. J. Newport, B. D. Rainford, and R. Cywinski (Hilger, Bristol, 1989).
- ²⁸G. L. Squires, *Introduction to the Theory of Thermal Neutron Scattering* (Cambridge University, Cambridge, 1978).
- ²⁹J. M. F. Gunn, in *Neutron Scattering at a Pulsed Source*, edited by R. J. Newport *et al.* (Hilger, Bristol, 1989).
- ³⁰A. K. Soper, W. S. Howells, and A. C. Hannon, Report RAL-89-046.
- ³¹G. Placzek, *Phys. Rev.* **86**, 377 (1952).
- ³²J. G. Powles, *Mol. Phys.* **36**, 623 (1979).
- ³³M. A. Howe, R. L. McGreevy, and W. S. Howells, *J. Phys. Condensed Matter* **1**, 3433 (1989).
- ³⁴P. B. Lukins, D. R. McKenzie, A. M. Vassallo, and J. V. Hanna, *Carbon* **31**, 569 (1993).
- ³⁵K. Yusada, H. Masuda, M. Takeda, and A. Yoshida, *Phys. Status Solidi a* **95**, 249 (1986).
- ³⁶A. R. Nyaicsh and W. B. Nowak, *J. Vac. Sci. Technol. A* **1**, 308 (1983).
- ³⁷W. B. Nowak (private communication).
- ³⁸J. Gonzalez-Hernandez, B. S. Chao, and D. A. Pawlik, *Mater. Sci. Forum*, **52/53**, 543 (1989).
- ³⁹S. Craig and G. L. Harding, *Thin Solid Films* **97**, 345 (1982).
- ⁴⁰P. Couderc and Y. Catherine, *Thin Solid Films* **146**, 93 (1987).
- ⁴¹D. R. McKenzie, R. C. McPhedran, N. Savvides, and L. C. Botton, *Philos. Mag. B* **48**, 341 (1983).
- ⁴²Y. Yin, R. E. Collins, and B. A. Pailthorpe, *J. Appl. Phys.* **71**, 3806 (1992).
- ⁴³F. W. Smith, *J. Appl. Phys.* **55**, 764 (1984).
- ⁴⁴S. Kumar, *Appl. Phys. Lett.* **58**, 1836 (1991).

The Journal of Chemical Physics is copyrighted by the American Institute of Physics (AIP). Redistribution of journal material is subject to the AIP online journal license and/or AIP copyright. For more information, see <http://ojps.aip.org/jcpo/jcpcr/jsp>
Copyright of Journal of Chemical Physics is the property of American Institute of Physics and its content may not be copied or emailed to multiple sites or posted to a listserv without the copyright holder's express written permission. However, users may print, download, or email articles for individual use.